aerospace

MDPI

Article

An Analytical Model for High-Velocity Impacts of Flaky Projectile on Woven Composite Plates

Chao Hang [1,*], Xiaochuan Liu [1], Yonghui Chen [1] and Tao Suo [2,*]

[1] National Key Laboratory of Strength and Structural Integrity, Aircraft Strength Research Institute of China, Xi'an 710065, China; liuxiaochuan@cae.ac.cn (X.L.); chen_yh623@163.com (Y.C.)
[2] School of Aeronautics, Northwestern Polytechnical University, Xi'an 710072, China
* Correspondence: hangchaonwpu@163.com (C.H.); suotao@nwpu.edu.cn (T.S.)

Abstract

Three-dimensional (3D) woven composites have good impact resistance and are expected to become the fan casing material for the next generation of turbofan engines. Conducting research on the performance of woven composite plates under high-velocity impact of flaky projectiles is of great significance for the containment design of the fan casing. Based on the principle of energy conservation, an analytical model for the high-velocity impact of flaky projectiles on carbon fiber woven composite plates was established for three typical failure modes: shear plugging, fiber failure, and momentum transfer. A segmented solution method combining analytical and numerical calculations was developed for the model. The critical penetration velocity of the plate obtained by the analytical method at different roll angles of the projectile is in good agreement with the experimental results, which verifies the accuracy of the analytical model. Moreover, the analytical results indicate that the critical penetration velocity of the plate increases first and then decreases with the roll angle of the projectile. Further energy conversion analysis points out that shear plugging is the main form of energy dissipation for woven composite plates, and the energy dissipation of shear plugging at a roll angle of 30° is higher than that at 0° and 60°. This elucidates the mechanism by which the roll angle of the projectile affects the critical penetration velocity of the plate from the perspective of energy dissipation.

Keywords: woven composite; analytical model; high-velocity impact; flaky projectile; roll angle

1. Introduction

Woven composites have become important materials for lightweight design of aerospace structures due to their low density and excellent mechanical properties [1–4]. Woven composites have good impact resistance and are expected to become a strong competitor for the fan casing material of next-generation engines [5–8]. In order to meet the containment requirements of the fan casing for detached blades, it is necessary to research the performance of woven composite plates under the high-velocity impact of flaky projectiles.

The internal structure of woven composite materials is complex, which brings many difficulties to the study of their performance under high-velocity impact of projectiles. At present, three methods are mainly used to investigate the high-velocity impact performance of woven composite plates: experiments, simulations, and analytical methods. In experiments, high-velocity projectiles are usually fired from air cannons or rifles to impact

Check for updates

Academic Editor: Changguo Wang

Received: 27 December 2025
Revised: 26 January 2026
Accepted: 27 January 2026
Published: 28 January 2026

Copyright: © 2026 by the authors. Licensee MDPI, Basel, Switzerland. This article is an open access article distributed under the terms and conditions of the Creative Commons Attribution (CC BY) license.

composite plates [9–13]. The simulation method requires establishing a finite element model for woven composites with complex internal structures [14–18]. The high-velocity impact deformation and failure behavior of plates are calculated by transient dynamic methods. However, neither experiment nor simulation methods are suitable for the preliminary design stage of impact resistance of woven composite plates due to their high cost and complex modeling process. Analytical methods have advantages in quickly predicting the critical penetration velocity of woven composite plates under high-velocity impact.

The analytical models of projectile impact on woven composite plates are mostly based on the principle of energy conservation. Gu [19] establishes an analytical model for high-velocity impact of a projectile on plain-woven fabrics, using a pyramid body to describe the failure zone of the plate and predicting the critical penetration velocity of the fabric well. Naik et al. [20] developed an analytical model for the high-velocity impact of cylindrical projectiles on two-dimensional glass fiber woven composite plates. Based on stress wave propagation theory, they distinguish the different energy dissipation forms of primary and secondary fiber bundles in the plates. This model can effectively predict the critical penetration velocity and damage size of the plates. Pasquali et al. [21] further developed Naik's analytical model, introducing the shear plugging failure form generated by the high-velocity impact of cylindrical projectiles on flat plates. This model has good predictive ability for the critical penetration velocity and damage size of carbon fiber and glass fiber plain woven composite plates. It has been shown that shear plugging failure is an important energy dissipation form of carbon fiber woven composite plates. Lopez et al. [22,23] established analytical models for high-velocity impact failure of carbon fiber plain woven composite plates using spherical and cylindrical projectiles based on the principle of energy conservation and the failure modes of woven composite plates. These models considered three energy dissipation mechanisms: plate crushing failure, fiber fracture, and momentum transfer. These models predict the residual velocity of the projectile well and discuss the influence of projectile mass and size on the residual velocity. Theoretical analysis also indicates that the energy dissipation of the plate's crushing failure is the highest when the initial velocity of the projectile is less than 300 m/s.

In high-velocity impact research under the background of casing containment, the flaky projectile is usually used to approximate the detached blades. However, the current analytical models [19–23] mainly focus on spherical and cylindrical projectiles and cannot be applied to the problem of high-velocity impact of flaky projectiles on woven composite plates.

In this paper, an analytical model for high-velocity impacts of flaky projectiles on carbon fiber woven composite plates based on the principle of energy conservation is proposed to investigate the influence of projectile roll angle on the critical penetration velocity and the impact energy dissipation mechanism of the plates. Our model advances existing energy-based ballistic limit formulations in two key ways. First, it explicitly introduces the projectile's roll angle as a continuous, independent variable, quantifying its effect on energy dissipation. Second, it generalizes the energy dissipation framework from the centrosymmetric failure modes typical of simple geometries (e.g., cylinders, spheres) to accommodate non-centrosymmetric damage patterns. An analytical model for high-velocity impacts of flaky projectiles is introduced in Section 2. The model solution method is presented in Section 3. The critical penetration velocity predicted by the analytical model is correlated with the experiments, and the parameter studies are discussed in Section 4 and briefly concluded in Section 5.

2. Analytical Model for High-Velocity Impact of Flaky Projectiles

The material investigated in this paper is a 3D woven composite fabricated from T800 carbon fibers and thermosetting epoxy resin, which was supplied by Weihai Guangwei Composites Co., Ltd. (Weihai, China). The fiber arrangement of the woven composite is illustrated in Figure 1. The manufacturing process mainly involves two steps: fiber preform fabrication and resin impregnation and curing. First, warp and weft fiber bundles are woven into fiber preforms according to a preset arrangement pattern using an automatic loom. Subsequently, the resin transfer molding (RTM) process is adopted to impregnate the fiber preforms with resin and conduct curing.

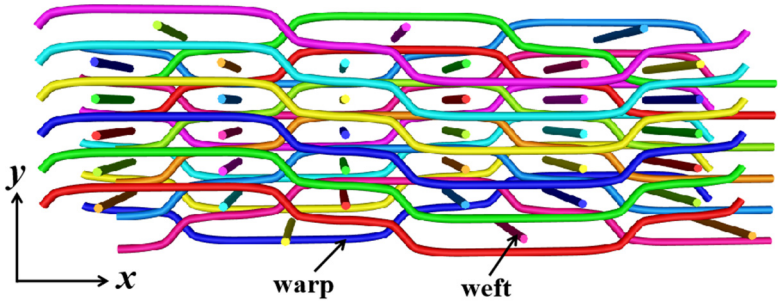


Figure 1. Fiber arrangement of the woven composite.

Figure 2 shows the typical failure modes of woven composite plates under high-velocity impact by a flaky projectile. The front of the plate undergoes neat shear failure, and the shear failure area is consistent with the cross-sectional shape of the projectile, which is a typical shear plugging failure. The back of the plate is mainly due to fiber tensile failure, with obvious cracks at the impact of the projectile and horizontal cracks at both ends of the projectile. The horizontal cracks are located in the cross-layer interlocking zone of the warp fiber bundles. When the flaky projectile impacts a plate with a roll posture, the region on the back of the plate affected by fiber tensile failure is approximately a parallelogram.

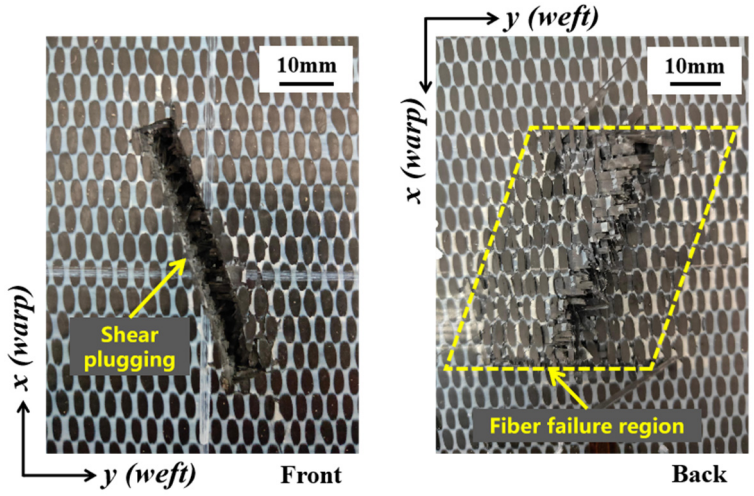


Figure 2. Typical failure modes of woven composite plates under flaky projectile impact.

Based on the high-velocity impact failure mode of woven composite plates, the analytical model considers three main energy dissipation forms of the plates: shear plugging, fiber failure, and momentum transfer. The energy dissipation of shear plugging corresponds to the neat punching and shearing failure of the front of the plate. Fiber failure energy dissipation corresponds to fiber tensile failure on the back of the plate. The momentum

transfer energy dissipation corresponds to the kinetic energy of the material accelerated by the projectile during the impact process.

The assumptions and limitations of the model are as follows: (1) The material failure mode is consistent with that illustrated in Figure 2. Since the model is derived based on the material's impact failure modes, it may not be directly extendable to composites with other microstructures. However, the modeling methodology proposed in this paper can provide a reference for their high-velocity impact research. (2) The projectile is assumed to be rigid, with no consideration of mass loss or structural damage. This assumption is applicable to penetration scenarios where the strength of the projectile is significantly higher than that of the target plate, and the impact velocity of the projectile should not be excessively high (e.g., below 250 m/s). (3) The rebound kinetic energy of the projectile is neglected since it is generally small. This simplification may introduce a minor error in the analysis of rebound conditions. (4) The strain rate effect of the material is neglected. This assumption is applicable to carbon/epoxy composites, as numerous studies have demonstrated that this material system is strain rate insensitive [24–26]. (5) The frictional energy dissipation between the projectile and the target plate is neglected. This assumption is applicable to projectiles with smooth surfaces. (6) The delamination damage of the composite is neglected. Given that it is highly challenging to incorporate the delamination behavior of woven composites into analytical models, the finite element method is an effective approach to address this limitation in future research [27,28].

Figure 3 is a schematic diagram of a high-velocity impact woven composite plate with a flaky projectile, showing the roll angle β between the projectile and the warp fiber bundles of the plate.

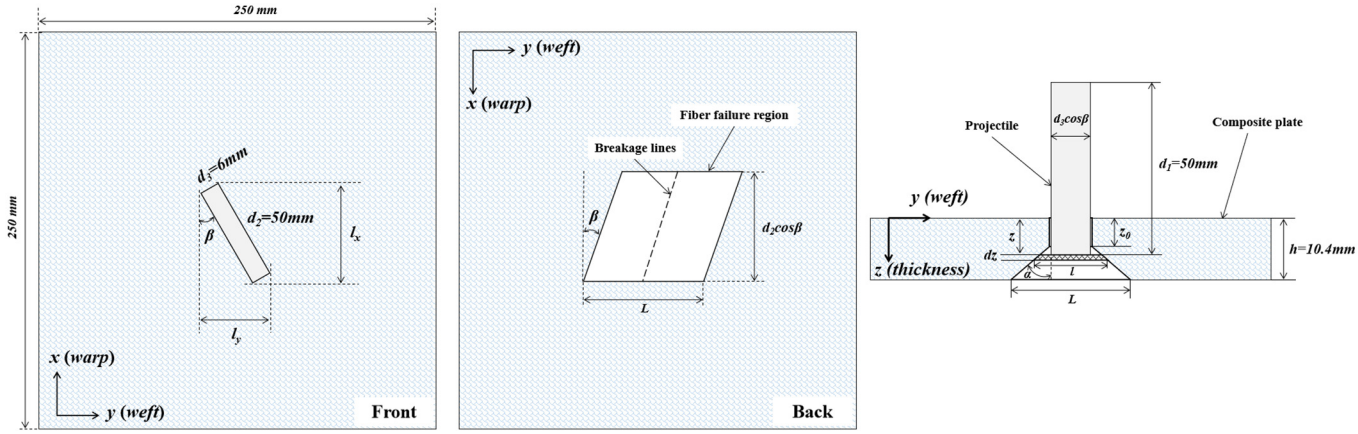


Figure 3. Schematic diagram of a high-velocity impact woven composite plate with a flaky projectile.

The projectile impacts the plate in the $+z$ direction at its initial velocity v_0. When a projectile impacts the composite plate and undergoes a small displacement dz, the energy conservation of the system can be expressed in the following differential form:

$$-\mathrm{d}E_k = \mathrm{d}E_{sp} + \mathrm{d}E_f + \mathrm{d}E_m \tag{1}$$

In Equation (1), E_k, E_{sp}, E_f, and E_m, respectively, represent the kinetic energy of the projectile, the plate energy dissipation of shear plugging, fiber fracture, and momentum transfer.

The differential form of projectile kinetic energy is as follows:

$$\mathrm{d}E_k(z) = \frac{1}{2} m_p \mathrm{d}(v(z)^2) \tag{2}$$

In Equation (2), m_p represents the mass of the projectile, and $v(z)$ represents the velocity of the projectile at coordinate z.

Shear plugging refers to the phenomenon where material at the front face of the target is sheared off by the edges of the projectile, as shown in Figure 2. The energy dissipated by shear plugging is proportional to the material's shear strength, the width of the fiber bundles subjected to shear failure, and the residual thickness of the target plate. The differential form of shear plugging energy dissipation in the impact zone of the plate is as follows:

$$\mathrm{d}E_{sp}(z) = 2(S_{xz}l_y + S_{yz}l_x)(h - z)\mathrm{d}z \tag{3}$$

In Equation (3), S_{xz} and S_{yz}, respectively, represent the out-of-plane shear strength of woven composites along the warp and weft directions. h represents the thickness of woven composite plates. l_x and l_y are the widths of the weft and warp fiber bundles subjected to shear failure, respectively, as illustrated in Figure 3. From the geometric relationship, it can be concluded that:

$$\begin{cases} l_x = d_2 \cos\beta + d_3 \sin\beta \\ l_y = d_2 \sin\beta + d_3 \cos\beta \end{cases} \tag{4}$$

For the sake of convenience, the following variables are defined as:

$$w_{sp} = 2(S_{xz}l_y + S_{yz}l_x) \tag{5}$$

Fiber failure refers to the observable fiber breakage on the rear face of the target, as shown in Figure 2. The energy dissipated by fiber failure is proportional to the material's fracture energy per unit volume and the volume of the fiber rupture zone. The differential form of energy dissipation for fiber failure on the back of the plate is as follows [22,23]:

$$\mathrm{d}E_f(z) = w_f \mathrm{d}V = \frac{1}{2}(X_t\varepsilon_f^x + Y_t\varepsilon_f^y)\mathrm{d}V \tag{6}$$

In Equation (6), w_f is the fiber failure energy per unit volume of woven composites. X_t and Y_t, respectively, represent the tensile strength of woven composites in the warp and weft directions. ε_f^x and ε_f^y, respectively, represent the tensile failure strain of woven composites in the warp and weft directions. $\mathrm{d}V$ represents the volume of material in the fiber failure zone. According to the geometric relationship in Figure 3, the length of the volume $\mathrm{d}V$ along the x direction is $d_2\cos\beta$, the length along the y direction is l, and the length along the z direction is dz. Therefore, its expression is as follows:

$$\begin{aligned} \mathrm{d}V &= l d_2 \cos\beta \mathrm{d}z \\ &= [d_3 \cos\beta + 2(z - z_0)\tan\alpha] d_2 \cos\beta \mathrm{d}z \\ &= [d_2 d_3 \cos^2\beta + 2(z - z_0) d_2 \cos\beta \tan\alpha] \mathrm{d}z \end{aligned} \tag{7}$$

In Equation (7), z_0 is the shear plugging depth of the projectile before fiber tensile failure occurs. α represents the expansion angle of the fiber failure zone. Lopez et al. [22,23] found that the expansion angle α formed by the high-velocity impact of a projectile on a carbon/epoxy woven composite plate is approximately 65°. For the composite investigated in this paper, the measured shear plugging failure depth on the front surface of the material in Figure 2 is 3.2 mm, and the width of the fiber fracture area on the back surface is 40.6 mm. Based on the geometric relationship shown in Figure 3, the expansion angle is calculated to be 67.6°, which is in good agreement with the results reported in the literature [22,23]. The influence of the expansion angle on the critical penetration velocity and energy dissipation of the plate will be discussed in detail in subsequent sections.

Considering that when fiber tensile failure occurs on the plate, the projectile has already generated a shear plug at a depth of z_0. It is necessary to define the following piecewise function to describe the effective range of energy dissipation for fiber tensile failure:

$$c_r(z) = \begin{cases} 0, 0 \le z \le z_0 \\ 1, z_0 < z \le h \\ 0, z > h \end{cases} \tag{8}$$

The physical meaning of applying the piecewise function to the fiber failure energy dissipation is as follows: when the projectile displacement is less than z_0, fiber failure does not occur; when the projectile displacement is between z_0 and h, energy dissipation due to fiber failure initiates; when the projectile displacement is greater than h, energy dissipation due to fiber failure ceases.

Momentum transfer refers to the phenomenon where material in the central region of the target is accelerated by the high-speed projectile and remains attached to it throughout the penetration process. The energy dissipated by momentum transfer is proportional to the mass of the accelerated material and the square of its velocity. The differential form of the energy dissipation for the momentum transfer of materials in the impact zone is as follows:

$$\mathrm{d}E_m(z) = \frac{1}{2}\rho d_2 d_3 v(z)^2 \mathrm{d}z \tag{9}$$

In Equation (9), ρ indicates the density of woven composites.

Substituting the expressions of the above four types of energy into Equation (1) yields the differential form of system energy conservation:

$$-\frac{1}{2}m_p \mathrm{d}(v(z)^2) = w_{sp}(h-z)\mathrm{d}z + w_f[d_2 d_3 \cos^2\beta + 2(z-z_0)d_2 \cos\beta \tan\alpha]\mathrm{d}z c_r(z) + \frac{1}{2}\rho d_2 d_3 v(z)^2 \mathrm{d}z \tag{10}$$

Analysis of the aforementioned equation reveals two unknown variables, $v(z)$ and z_0, which cannot be solved directly and thus require additional constraint conditions. As reported in the literature [29], based on impact simulation results, no significant out-of-plane deformation of the plate occurs during the initial impact stage, whereas a punch-shear pit with a depth of z_0 forms on the plate's front surface. The duration of this initial stage is approximately equivalent to the time required for the stress wave to propagate back and forth along the plate's thickness direction. In the second stage of impact, the plate begins to undergo fiber tensile failure. Therefore, equations regarding $v(z)$ and z_0 can be established:

$$\int_0^{z_0} \frac{\mathrm{d}z}{v(z)} = \frac{2h}{\sqrt{E_z/\rho}} \tag{11}$$

In the equation, E_z indicates the elastic modulus of woven composites in the thickness direction.

At this point, the analytical model for high-velocity impacts of flaky projectiles on woven composite plates has been established. Simultaneously, Equations (10) and (11) can be used to solve for $v(z)$ and z_0, and the specific solution process will be discussed in the next section.

3. Model Solution Method

Based on the initial conditions of the high-velocity impact problem, Equation (10) can be written in the following form:

$$\begin{cases} -\frac{1}{2}m_p \frac{\mathrm{d}v^2}{\mathrm{d}z} = w_{sp}(h-z) + w_f[d_2 d_3 \cos^2\beta + 2(z-z_0)d_2 \cos\beta \tan\alpha]c_r + \frac{1}{2}\rho d_2 d_3 v^2 \\ v(0) = v_0 \end{cases} \tag{12}$$

For ease of solution, the variables are dimensionless:

$$v^* = \frac{v}{v_0}, z^* = \frac{z}{h}, z_0^* = \frac{z_0}{h} \tag{13}$$

Define variables $w^* = v^{*2}$, then Equations (12) and (11) are transformed into the following forms, respectively:

$$\begin{cases} -\frac{\mathrm{d}w^*}{\mathrm{d}z^*} = \frac{2h^2 w_{sp}}{m_p v_0^2}(1 - z^*) + \frac{2hw_f d_2 d_3 \cos^2\beta}{m_p v_0^2}[1 + \frac{2h\tan\alpha}{d_3\cos\beta}(z^* - z_0^*)]c_r + \frac{\rho d_2 d_3 h}{m_p} w^* \\ w^*(0) = 1 \end{cases} \tag{14}$$

$$\int_0^{z_0^*} \frac{h}{v_0\sqrt{w^*(z^*)}}\mathrm{d}z^* = \frac{2h}{\sqrt{E_z/\rho}} \tag{15}$$

In order to make the expression concise and distinguish the three forms of energy dissipation of the plate, the following variables are defined as follows:

$$\begin{cases} R_{sp} = \frac{2h^2 w_{sp}}{m_p v_0^2} \\ R_f = \frac{2hw_f d_2 d_3 \cos^2\beta}{m_p v_0^2} \\ R_m = \frac{\rho d_2 d_3 h}{m_p} \end{cases} \tag{16}$$

Considering the special properties of the $c_r(z)$ function, Equation (14) can be simplified as follows when $0 \le z^* \le z_0^*$:

$$\begin{cases} -\frac{\mathrm{d}w^*}{\mathrm{d}z^*} = R_{sp}(1 - z^*) + R_m w^*, 0 \le z^* \le z_0^* \\ w^*(0) = 1 \end{cases} \tag{17}$$

The above equation is a first-order linear differential equation, and its analytical solution can be obtained as follows:

$$w^* = e^{-R_m z^*}\left(\frac{R_{sp}}{R_m^2} + \frac{R_{sp}}{R_m} + 1\right) + \frac{R_{sp}}{R_m}z^* - \frac{R_{sp}}{R_m^2} - \frac{R_{sp}}{R_m}, 0 \le z^* \le z_0^* \tag{18}$$

Substituting Equation (18) into Equation (15), z_0 can be calculated numerically. Substitute z_0 into Equation (14) and use the 4th order Runge—Kutta method to obtain the numerical solution for w^* within the range $z_0^* < z^* \le 1$.

By combining analytical and numerical methods to solve the above equation, the projectile velocity $v(z)$ can be obtained. When $v(h) = 0$, the initial impact velocity of the projectile is the critical penetration velocity V_{50} of the plate.

Based on the above results, each type of energy dissipation of the plate can be solved, which is used to investigate the energy dissipation mechanism of the plate. The kinetic energy of the projectile is as follows:

$$E_k(z) = \frac{1}{2}m_p v(z)^2 = \frac{1}{2}m_p w^*\left(\frac{z}{h}\right)^2 \tag{19}$$

The energy dissipation of shear plugging in the impact zone of the plate satisfies the following equation:

$$\begin{cases} -\frac{\mathrm{d}E_{sp}(z)}{\mathrm{d}z} = w_{sp}(h - z) \\ E_{sp}(0) = 0 \end{cases} \tag{20}$$

By solving the above equation, it can be concluded that:

$$E_{sp}(z) = -\frac{1}{2}w_{sp}z^2 + hw_{sp}z \tag{21}$$

The energy dissipation of fiber failure on the back of the plate meets the following equation:

$$\begin{cases} -\frac{dE_f(z)}{dz} = w_f[d_2d_3\cos^2\beta + 2(z-z_0)d_2\cos\beta\tan\alpha]c_r(z) \\ E_f(0) = 0 \\ E_f(z_0) = 0 \end{cases} \tag{22}$$

By solving the above equation, it can be concluded that:

$$E_f(z) = \begin{cases} 0, 0 \le z \le z_0 \\ t_2z^2 + (t_1 - 2z_0t_2)z + t_2z_0^2 - t_1z_0, z_0 < z \le h \end{cases} \tag{23}$$

In the equation:

$$\begin{cases} t_1 = w_fd_2d_3\cos^2\beta \\ t_2 = w_fd_2\cos\beta\tan\alpha \end{cases} \tag{24}$$

The energy dissipation of momentum transfer in the plate impact zone satisfies the following equation:

$$\begin{cases} -\frac{dE_m(z^*)}{dz^*} = \frac{1}{2}h\rho d_2d_3v_0^2w^*(z^*) \\ E_m(0) = 0 \end{cases} \tag{25}$$

Due to the lack of analytical solutions for w^* within the range $z_0^* < z^* \le 1$, only numerical solutions are available. Therefore, the numerical solution for E_m can only be obtained through numerical methods.

The total energy of the system is E_0, and the corresponding dimensionless energy for each type of energy is as follows:

$$E_0 = \frac{1}{2}m_pv_0^2,\ \mathrm{E}_k^* = \frac{E_k}{E_0}, E_{sp}^* = \frac{E_{sp}}{E_0},\ \mathrm{E}_f^* = \frac{E_f}{E_0},\ \mathrm{E}_m^* = \frac{E_m}{E_0} \tag{26}$$

4. Results and Discussion

4.1. Model Verification

In order to verify the accuracy of the high-velocity impact model proposed in this work, the critical penetration velocity of woven composite plates measured by high-velocity impact experiments is compared with the predicted results of the model. The air cannon system is employed to carry out experiments on the impact of flaky projectiles on woven composite plates. The experimental principle is depicted in Figure 4, wherein a high-speed camera is utilized to measure the initial velocity of the projectile impacting the plate. The projectile material is TC4 titanium alloy, with dimensions of 50 mm × 50 mm × 6 mm and a mass of 66 g. The test piece is a carbon/epoxy 3D woven composite plate with dimensions of 250 mm × 250 mm × 10.4 mm. The projectile's initial velocity is adjusted via the up–down method until it embeds in the woven composite plate. This velocity is then defined as the critical penetration velocity. By adjusting the angle of the plate using the fixture, the critical penetration velocity of the plate under different roll angle conditions can be obtained.

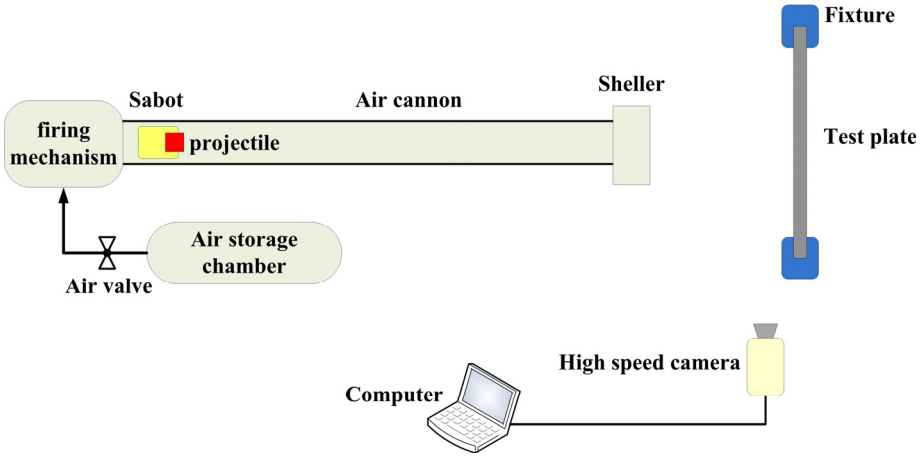


Figure 4. Principle of high-velocity impact experiments.

A series of high-velocity impact tests with different roll angles and projectile initial velocities was conducted, and the results are presented in Table 1. The results of the first four tests correspond to projectile embedment, whose projectile initial velocities match the critical penetration velocities of the target plates. The failure modes of the target plates at the critical penetration velocities are illustrated in Figure 5.

Table 1. High-velocity impact test results.

Test Number	Roll Angle β	V_0 (m/s)	Result
a	7°	155.3	Embedment
b	28°	155.7	Embedment
c	50°	146.2	Embedment
d	62°	140.0	Embedment
e	0°	152.2	Rebound
f	26°	145.5	Rebound
g	10°	156.8	Penetration
h	21°	179.8	Penetration
i	23°	170.7	Penetration
j	66°	153.8	Penetration

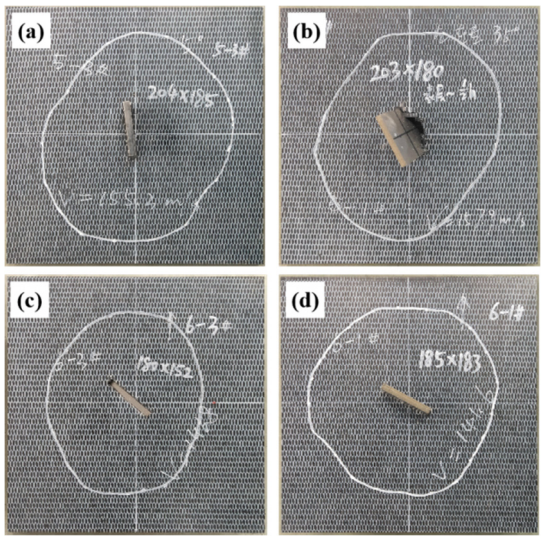


Figure 5. Failure modes of plates at the critical penetration velocities: (**a**) roll angle 7°; (**b**) roll angle 28°; (**c**) roll angle 50°; (**d**) roll angle 62°.

The critical penetration velocity of the plate can be predicted by substituting the mechanical properties of the woven composite plate, shown in Table 2, into the analytical model. Figure 6 presents the model-predicted critical penetration velocity and the high-velocity impact test results. The predicted critical penetration velocities show excellent agreement with those obtained from the embedment case tests, with the relative errors all within 3% across the four roll angles. Furthermore, the model-predicted critical penetration velocity curve separates the vast majority of the rebound and penetration experimental data points on either side of the curve. The accuracy of the analytical model is thus fully validated. At the same time, the analytical results also indicate that the critical penetration velocity of the plate first increases and then decreases when the roll angle of the projectile is within the range of 0° to 70°. The critical penetration velocity of the plate reaches the maximum value of 156.9 m/s when the roll angle of the projectile is 22°. Considering that the angle in real engines between the tip of the fan blade and the circumferential direction of the casing is generally in the range of 20° to 30°, the impact resistance advantage of 3D woven composite can be fully utilized.

Table 2. Mechanical properties of the woven composite plate [29,30].

ρ (kg/m^3)	E_z (GPa)	X_t (MPa)	Y_t (MPa)	S_{xz} (MPa)	S_{yz} (MPa)	ε_f^x	ε_f^y
1526	9.2	407.1	1076.8	41.1	108.7	1.25%	1.36%

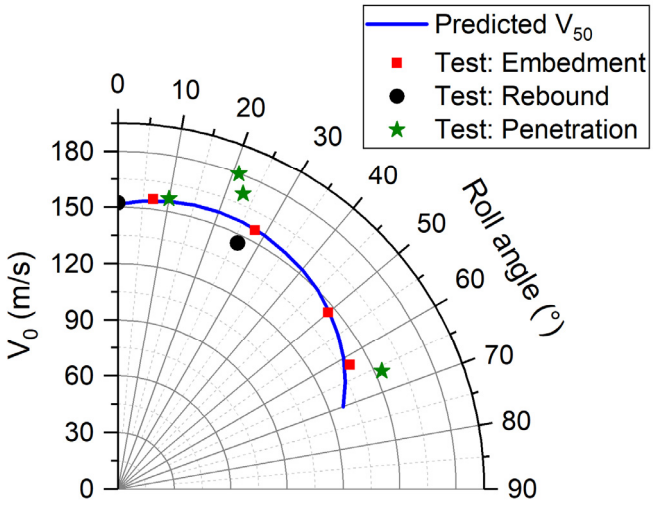


Figure 6. Critical penetration velocity predicted by the model and high-velocity impact test results.

4.2. Discussion on Energy Conversion During Impact Processes

Figures 7–9 illustrate the variation trends of dimensionless and absolute energies with dimensionless displacement under three typical roll angles (0°, 30°, and 60°) and varying impact velocities. As the displacement of the projectile increases, the kinetic energy of the projectile gradually decreases, while the three types of energy dissipation of the plate, namely shear plugging, fiber failure, and momentum transfer, continue to increase. The energy change trend during the impact process remains consistent across three tested roll angles and three initial velocities. This suggests that the roll angle and initial velocity of the projectile have no significant effect on the energy dissipation mechanism of the plate.

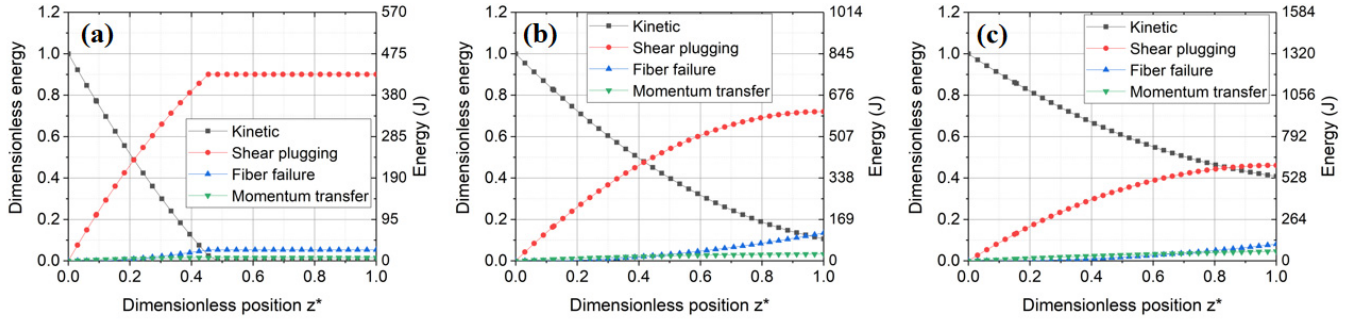


Figure 7. Energy-displacement curve at 0°: (**a**) v_0 = 120 m/s; (**b**) v_0 = 160 m/s; (**c**) v_0 = 200 m/s.

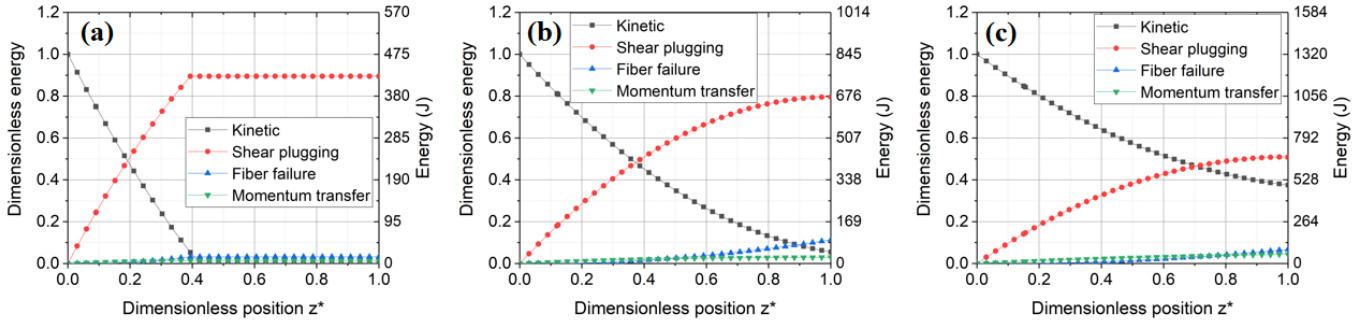


Figure 8. Energy-displacement curve at 30°: (**a**) v_0 = 120 m/s; (**b**) v_0 = 160 m/s; (**c**) v_0 = 200 m/s.

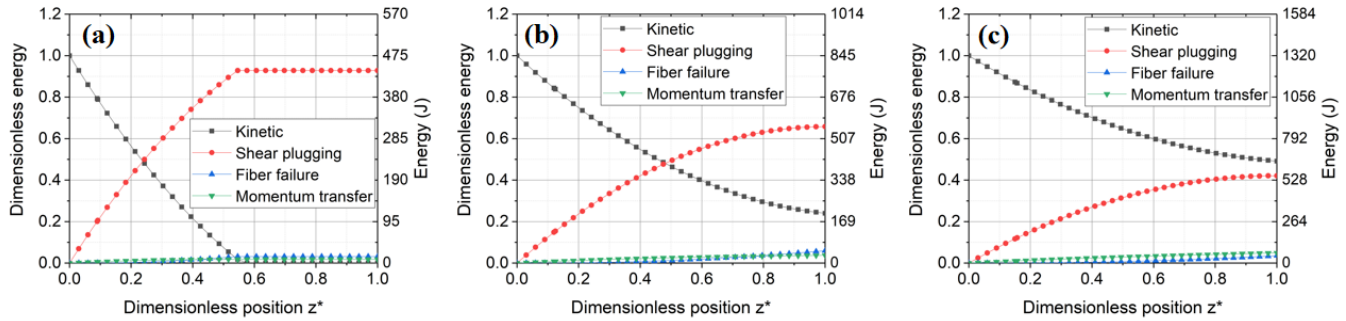


Figure 9. Energy-displacement curve at 60°: (**a**) v_0 = 120 m/s; (**b**) v_0 = 160 m/s; (**c**) v_0 = 200 m/s.

As the initial velocity of the projectile increases, the residual kinetic energy of the projectile also gradually increases. In real impact tests, if the projectile's initial velocity is below the plate's critical penetration velocity, the projectile rebounds. Notably, it retains a non-zero residual velocity in this scenario. The projectile's rebound kinetic energy is typically minimal. Therefore, this study's model neglects it, assuming that all projectile kinetic energy is converted into flat plate energy dissipation during rebound. This simplification process has no effect on the residual kinetic energy of the projectile under the conditions of projectile embedding and penetration.

Throughout the impact process, the plate's shear plugging energy dissipation dominates over the other two energy dissipation mechanisms. This indicates that the projectile's kinetic energy is primarily dissipated as shear plugging energy. Therefore, the shear plugging energy dissipation is the most important factor determining the critical penetration velocity of the plate.

4.3. Discussion on Energy Dissipation Under Different Impact Conditions

Figure 10 presents the variation in the projectile's residual kinetic energy and the three types of energy dissipated by the plate with the initial impact velocity. These energies include

both dimensionless and absolute energy values. Below the critical penetration velocity, the shear plugging energy dissipation increases gradually with the impact velocity, while its proportion remains approximately constant. At this stage, the fiber fracture and momentum transfer energy dissipation increase progressively with the impact velocity. However, when the impact velocity exceeds the critical penetration velocity, the projectile's residual kinetic energy and momentum transfer energy dissipation increase with the impact velocity. As the impact velocity increases, the proportion of energy dissipation caused by shear plugging and fiber failure gradually decreases, while the absolute values of these two energies remain nearly unchanged. This indicates that the energy dissipation caused by shear plugging and fiber failure is less affected by the projectile's impact velocity in the case of penetration.

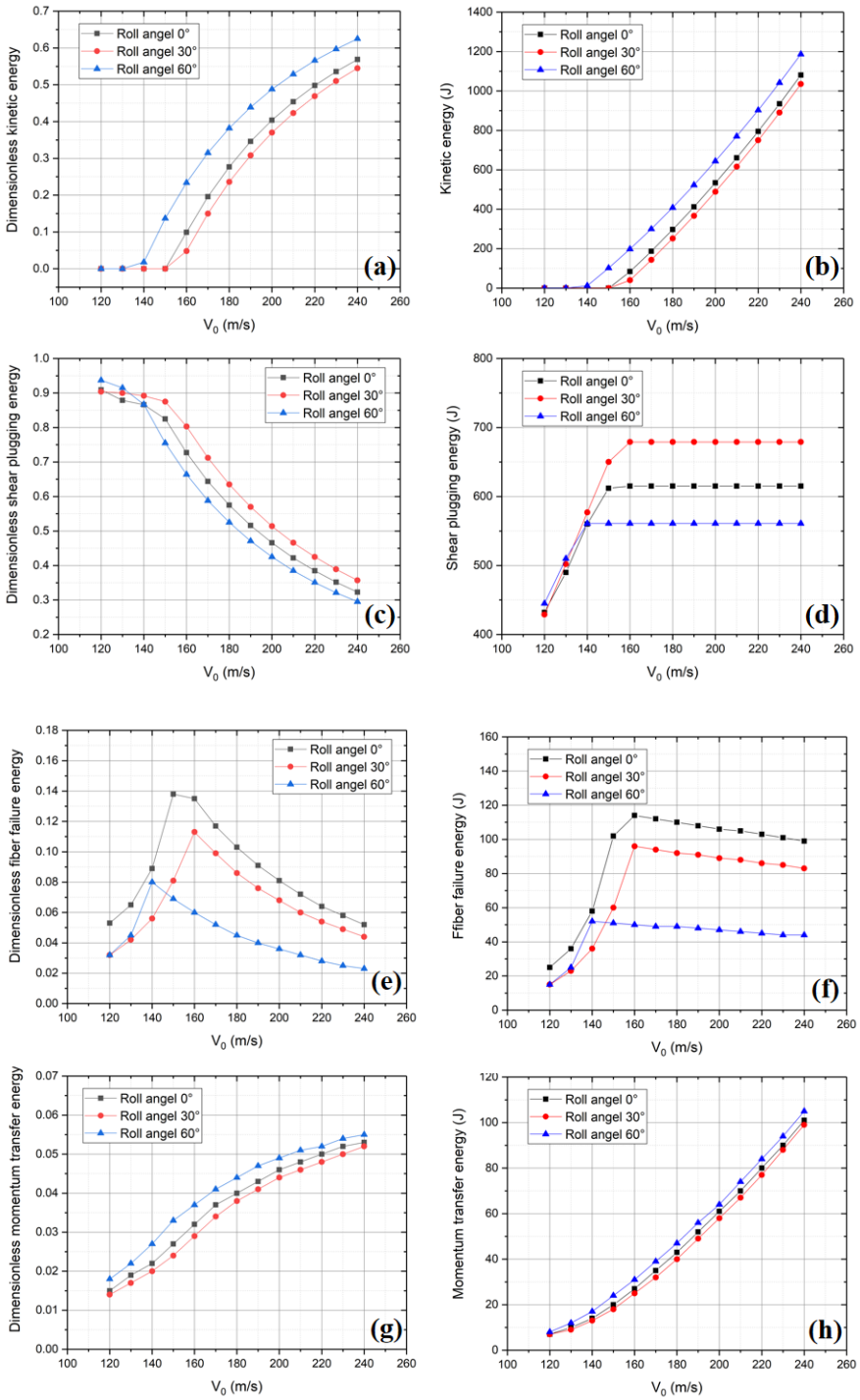


Figure 10. Energy-impact initial velocity curve: (**a**) E_k^*; (**b**) E_k; (**c**) E_{sp}^*; (**d**) E_{sp}; (**e**) E_f^*; (**f**) E_f; (**g**) E_m^*; (**h**) E_m.

Within the projectile impact velocity range of 120 m/s to 240 m/s, three different energy dissipation mechanisms were compared. The energy dissipation associated with shear plugging is significantly higher than that from fiber failure and momentum transfer, making it the dominant energy dissipation mechanism. Moreover, the shear plugging energy with a roll angle of 30° is higher than that at 0° and 60°, respectively. The shear plugging energy dissipation of the plate is closely related to the number of fiber bundles that undergo shear failure. As the roll angle of the projectile increases from 0°, the number of warp fiber bundles that undergo shear failure gradually increases, while the number of weft fiber bundles first slightly increases and then decreases. Given that the strength of weft fiber bundles in woven composites is higher than that of warp fiber bundles, the shear plugging energy dissipation increases first and then decreases with the projectile roll angle. Due to the dominant role of shear plugging energy dissipation, the projectile roll angle exhibits the same trend of influence on the critical penetration velocity of the plate. The peak value of the critical penetration velocity corresponds to the roll attitude where the projectile edge exerts shear action on a larger number of weft fiber bundles (the primary load-bearing fiber bundles).

4.4. Influence of Expansion Angle

The expansion angle is a key parameter characterizing the failure region during material fracture. It affects the volume of the fiber fracture region and thus the calculation of energy dissipation. Figure 11 presents the variation trend of the critical penetration velocity of plates under different expansion angles. For any fixed projectile roll angle, the V_{50} of the plate increases monotonically with the increase in the expansion angle. Within the expansion angle range of 55° to 75°, the variation range of V_{50} is less than 10 m/s, and the V_{50} prediction error induced by adopting a 65° expansion angle is less than 4.4%. Within the range of 60° to 70°, the V_{50} prediction error associated with a 65° expansion angle is less than 1.8%. This indicates that the model exhibits a certain degree of robustness with respect to the selection of the expansion angle.

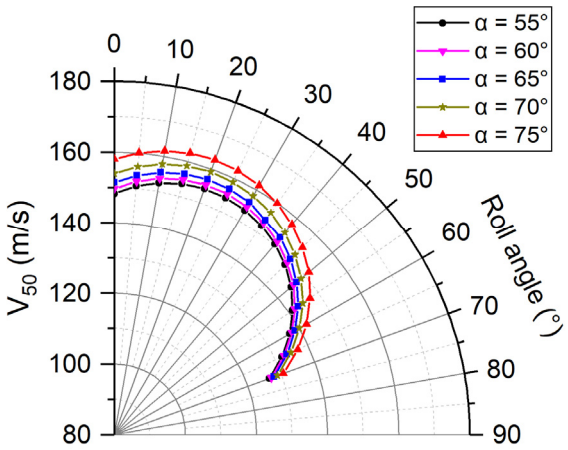


Figure 11. Variation in critical penetration velocity with respect to expansion angle.

A typical projectile roll angle of 30° is selected to analyze the influence of each energy dissipation component on the expansion angle under different impact velocities (120 m/s for the rebound condition and 180 m/s for the penetration condition). The results are illustrated in Figure 12. Under both conditions, the expansion angle has a negligible effect on shear plugging and momentum transfer energy dissipation and does not alter the dominant position of shear plugging energy dissipation. Fiber failure energy dissipation increases with the enlargement of the expansion angle, and this growth is particularly

pronounced under penetration conditions. This is because a larger expansion angle corresponds to a larger fiber tensile failure region, leading to more fiber tensile fractures for energy absorption.

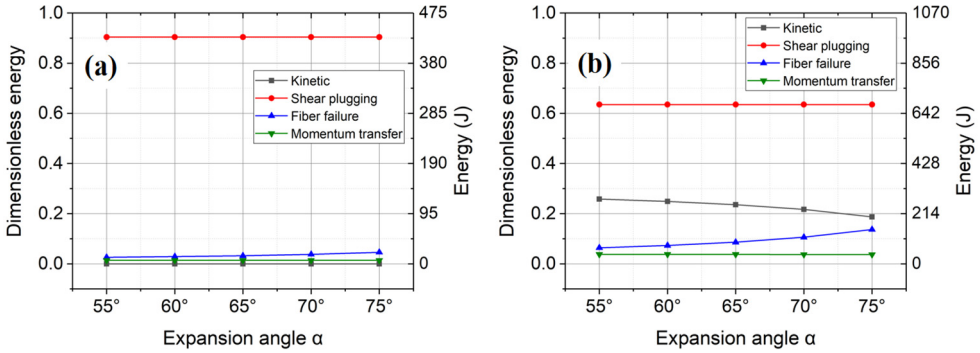


Figure 12. Variation in projectile residual kinetic energy and plate energy dissipation with respect to expansion angle: (**a**) v_0 = 120 m/s; (**b**) v_0 = 180 m/s.

4.5. Influence of Target Plate Thickness

Analyzing the influence of target plate thickness on the critical penetration velocity and energy absorption mechanisms is crucial for the lightweight design of composite protective structures. Figure 13 presents the variation trend in critical penetration velocity under different target plate thicknesses. For all projectile roll angles, the V_{50} increases with an increase in target plate thickness, exhibiting an approximately linear growth relationship. For instance, at a projectile roll angle of 30°, when the thickness increases from 9.4 mm to 11.4 mm, V_{50} rises from 141.2 m/s to 170.8 m/s, with a growth rate of 14.8 (m/s)/mm. This intuitively demonstrates that increasing thickness is a direct and effective means to enhance the impact resistance of woven composite plates.

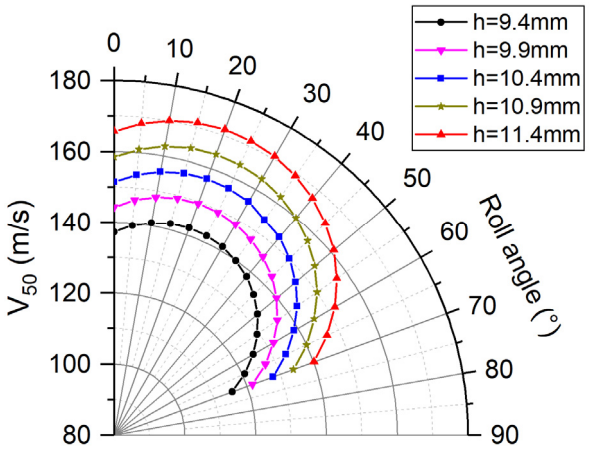


Figure 13. Variation in critical penetration velocity with respect to target plate thickness.

A typical projectile roll angle of 30° is selected to analyze the evolution of energy dissipation with target plate thickness under different impact velocities (120 m/s for the rebound condition and 180 m/s for the penetration condition). The results are illustrated in Figure 14. Under the rebound condition, target plate thickness has a minor effect on energy dissipation. Under the penetration condition, an increase in target plate thickness significantly enhances shear plugging, the dominant energy dissipation mechanism, while also promoting fiber failure energy dissipation. This is because an increase in target plate thickness directly expands the scope of the shear plugging and fiber fracture regions. The combined effect of these two energy dissipation forms leads to a significant increase in

the V_{50} of the plate. From the perspective of projectile residual kinetic energy under the penetration condition, its value decreases sharply with increasing thickness, which intuitively verifies the important role of thickness in dissipating projectile kinetic energy.

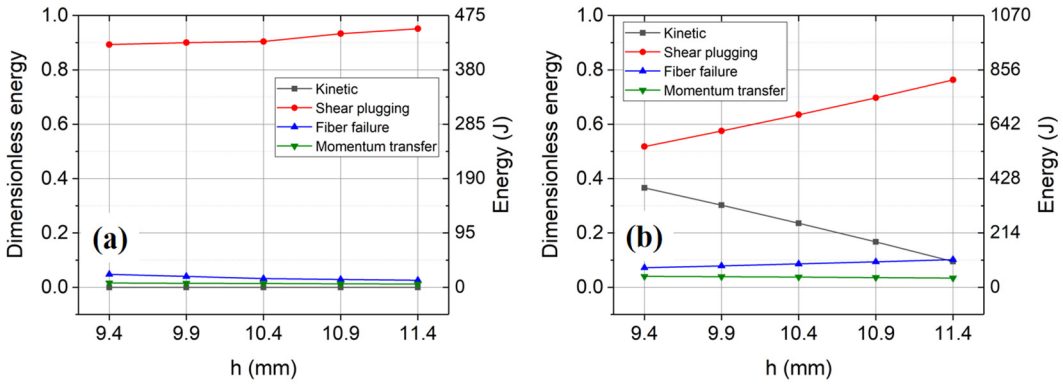


Figure 14. Variation in projectile residual kinetic energy and plate energy dissipation with respect to target plate thickness: (**a**) v_0 = 120 m/s; (**b**) v_0 = 180 m/s.

4.6. Influence of Projectile Geometry

Analyzing the influence of projectile geometric dimensions is of great significance for evaluating the protective capability of target plates against threats of different levels.

Figure 15 presents the variation trend of critical penetration velocity under different projectile thicknesses. For all projectile roll angles, the V_{50} decreases monotonically with the increase in projectile thickness. For instance, at a projectile roll angle of 30°, when the projectile thickness increases from 5 mm to 7 mm, V_{50} decreases from 169.2 m/s to 145.8 m/s, with a decrease rate of 11.7 (m/s)/mm. This trend is completely opposite to that of the target plate thickness. It indicates that projectiles with larger thickness possess stronger penetration capability. The decreasing rate of V_{50} gradually slows down with the increase in projectile thickness, exhibiting a certain degree of nonlinearity. This implies that the influence of projectile thickness on impact resistance has a marginal effect.

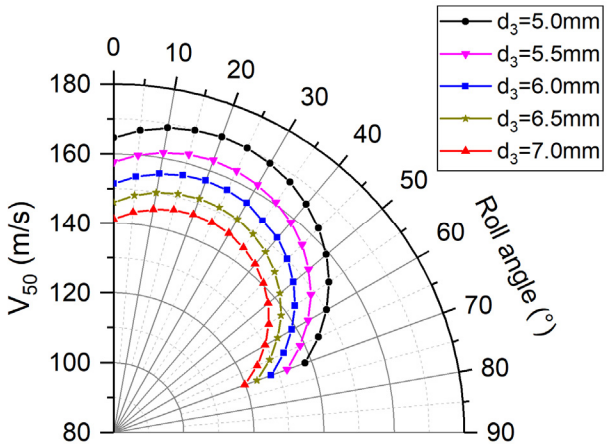


Figure 15. Variation in critical penetration velocity with respect to target projectile thickness.

A typical projectile roll angle of 30° is selected to analyze the evolution of energy dissipation with projectile thickness under different impact velocities (120 m/s for the rebound condition and 180 m/s for the penetration condition). The results are illustrated in Figure 16. Under both impact conditions, the absolute values of shear plugging and fiber failure energy dissipation increase with projectile thickness. This is because an increase in projectile thickness directly expands the scope of the shear plugging and fiber fracture

regions. However, an increase in projectile thickness leads to a faster growth rate of the projectile's initial kinetic energy. This explains why the V_{50} decreases with increasing projectile thickness.

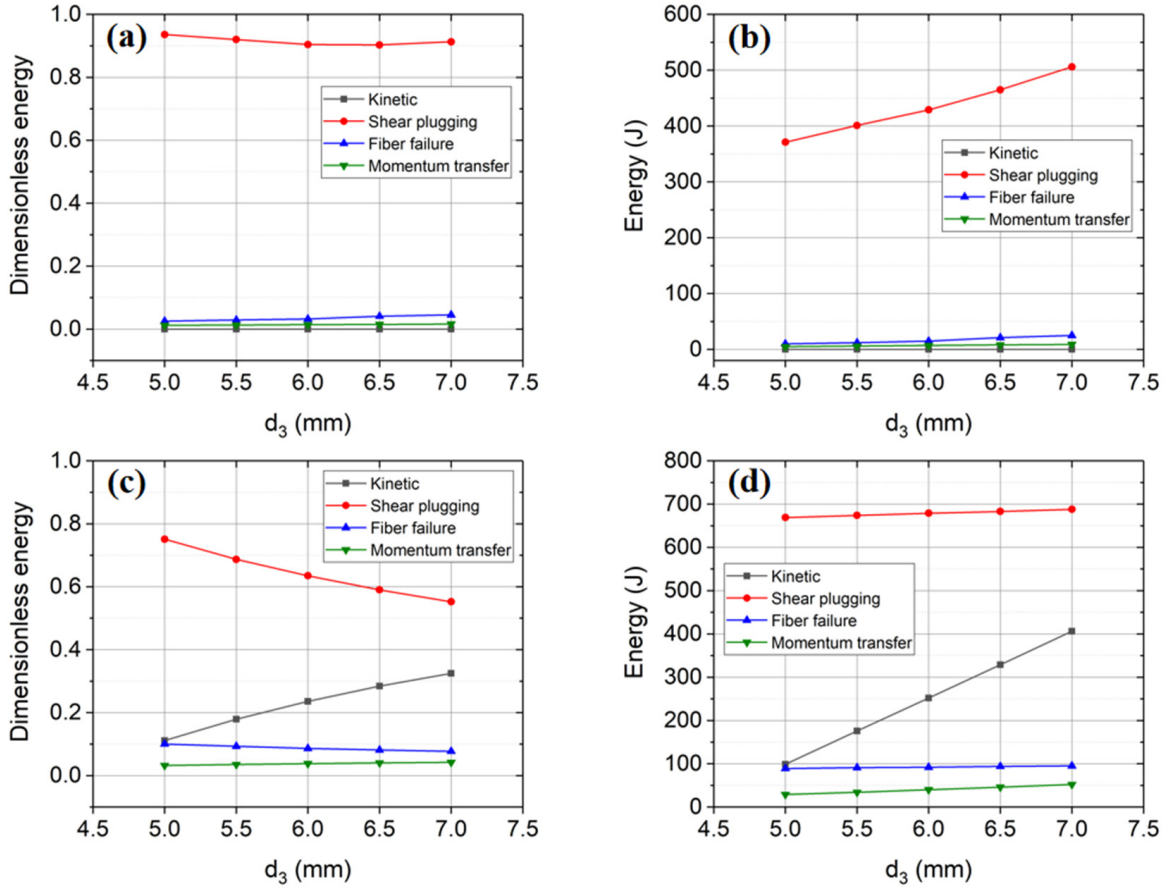


Figure 16. Variation in projectile residual kinetic energy and plate energy dissipation with respect to projectile thickness: (**a**) v_0 = 120 m/s; (**b**) v_0 = 120 m/s; (**c**) v_0 = 180 m/s; (**d**) v_0 = 180 m/s.

5. Conclusions

Based on the principle of energy conservation, an analytical model for the high-velocity impact of a flaky projectile on woven composite plates is established, which effectively predicts the critical penetration velocity of the plate under different roll angles of the projectile. Analysis reveals that shear plugging dominates energy dissipation in woven composite plates. At a projectile roll angle of 30°, shear plugging exhibits higher dissipation compared to 0° and 60°, explaining the non-monotonic variation in the plate's critical penetration velocity—first increasing and then decreasing with the roll angle. Parametric studies indicate that the expansion angle affects the V_{50} by regulating the scale of fiber failure. The larger the target plate thickness, the higher the dominant shear plugging energy dissipation of the plate, which effectively enhances its impact resistance. In contrast, the projectile thickness reduces the V_{50} by rapidly increasing the impact kinetic energy. The analytical model developed in this article has guiding significance for the containment design of composite fan casings.

Author Contributions: Conceptualization, C.H. and T.S.; methodology, C.H. and X.L.; software, C.H.; validation, C.H. and Y.C.; formal analysis, C.H.; investigation, C.H.; resources, X.L. and T.S.; data curation, C.H. and Y.C.; writing—original draft preparation, C.H.; writing—review and editing, C.H., X.L. and T.S.; funding acquisition, X.L. and T.S. All authors have read and agreed to the published version of the manuscript.

Funding: This research was funded by the Independent Research Project of the National Key Laboratory of Strength and Structural Integrity [grant number BYST-QZSYS-25-019-7]; the National Key R&D Program of China [grant number 2023YFB3709805] and the National Science and Technology Major Project [grant number2017-VII-0011].

Institutional Review Board Statement: Not applicable.

Informed Consent Statement: Not applicable.

Data Availability Statement: The original contributions presented in this study are included in the article. Further inquiries can be directed to the corresponding author.

Conflicts of Interest: The authors declare no conflicts of interest.

References

1. Marsh, G. Aero engines lose weight thanks to composites. *Reinf. Plast.* **2012**, *56*, 32–35. [CrossRef]
2. Zhang, X.; Chen, Y.; Hu, J. Recent advances in the development of aerospace materials. *Prog. Aerosp. Sci.* **2018**, *97*, 22–34. [CrossRef]
3. Mouritz, A.P.; Bannister, M.K.; Falzon, P.J.; Leong, K.H. Review of applications for advanced three-dimensional fibre textile composites. *Compos. Part A Appl. Sci. Manuf.* **1999**, *30*, 1445–1461. [CrossRef]
4. Sadighi, M.; Alderliesten, R. Impact fatigue, multiple and repeated low-velocity impacts on FRP composites: A review. *Compos. Struct.* **2022**, *297*, 115962. [CrossRef]
5. Li, Y.; Chen, X.; Zhou, J.; Liu, X.; Zhang, D.; Du, F.; He, W.; Jia, P.; Liu, H. A review of high-velocity impact on fiber-reinforced textile composites: Potential for aero engine applications. *Int. J. Mech. Syst. Dyn.* **2022**, *2*, 50–64. [CrossRef]
6. Falaschetti, M.P.; Semprucci, F.; Hernández, J.B.; Troiani, E. Experimental and Numerical Assessment of Crashworthiness Properties of Composite Materials: A Review. *Aerospace* **2025**, *12*, 122. [CrossRef]
7. Saboktakin, A. 3D textile preforms and composites for aircraft structures: A review. *Int. J. Aviat. Aeronaut. Aerosp.* **2019**, *6*, 2.
8. Huang, T.; Wang, Y.; Wang, G. Review of the Mechanical Properties of a 3D Woven Composite and Its Applications. *Polym. Technol. Eng.* **2017**, *57*, 740–756. [CrossRef]
9. Carney, K.S.; Pereira, J.M.; Revilock, D.M.; Matheny, P. Jet engine fan blade containment using an alternate geometry. *Int. J. Impact Eng.* **2009**, *36*, 720–728. [CrossRef]
10. Sevkat, E. Experimental and numerical approaches for estimating ballistic limit velocities of woven composite beams. *Int. J. Impact Eng.* **2012**, *45*, 16–27. [CrossRef]
11. Muñoz, R.; Martínez-Hergueta, F.; Gálvez, F.; González, C.; Llorca, J. Ballistic performance of hybrid 3D woven composites: Experiments and simulations. *Compos. Struct.* **2015**, *127*, 141–151. [CrossRef]
12. Reddy, P.; Reddy, T.S.; Madhu, V.; Gogia, A.; Rao, K.V. Behavior of E-glass composite laminates under ballistic impact. *Mater. Des.* **2015**, *84*, 79–86. [CrossRef]
13. Roberts, G.D.; Pereira, J.M.; Revilock, D.M.; Binienda, W.K.; Xie, M.; Braley, M. Ballistic Impact of Braided Composites with a Soft Projectile. *J. Aerosp. Eng.* **2004**, *18*, 3–7. [CrossRef]
14. Ma, P.; Jin, L.; Wu, L. Experimental and numerical comparisons of ballistic impact behaviors between 3D angle-interlock woven fabric and its reinforced composite. *J. Ind. Text.* **2019**, *48*, 1044–1058. [CrossRef]
15. Chocron, S.; Carpenter, A.J.; Scott, N.; Bigger, R.P.; Warren, K. Impact on carbon fiber composite: Ballistic tests, material tests, and computer simulations. *Int. J. Impact Eng.* **2019**, *131*, 39–56. [CrossRef]
16. Jia, X.; Sun, B.; Gu, B. Ballistic penetration of conically cylindrical steel projectile into 3D orthogonal woven composite: A finite element study at microstructure level. *J. Compos. Mater.* **2011**, *45*, 965–987.
17. Liu, Y.; Si, X.; Liu, P.; Zhang, X. Mesoscopic modeling and simulation of 3D orthogonal woven composites using material point method. *Compos. Struct.* **2018**, *203*, 425–435. [CrossRef]
18. Luan, K.; Sun, B.; Gu, B. Ballistic impact damages of 3-D angle-interlock woven composites based on high strain rate constitutive equation of fiber tows. *Int. J. Impact Eng.* **2013**, *57*, 145–158. [CrossRef]
19. Gu, B. Analytical modeling for the ballistic perforation of planar plain-woven fabric target by projectile. *Compos. Part B Eng.* **2003**, *34*, 361–371. [CrossRef]
20. Naik, N.K.; Shrirao, P.; Reddy, B.C.K. Ballistic impact behaviour of woven fabric composites: Formulation. *Int. J. Impact Eng.* **2006**, *32*, 1521–1552. [CrossRef]
21. Pasquali, M.; Terra, C.; Gaudenzi, P. Analytical modelling of high-velocity impacts on thin woven fabric composite targets. *Compos. Struct.* **2015**, *131*, 951–965. [CrossRef]
22. López-Puente, J.; Zaera, R.; Navarro, C. An analytical model for high velocity impacts on thin CFRPs woven laminated plates. *Int. J. Solids Struct.* **2007**, *44*, 2837–2851. [CrossRef]

23. López-Puente, J.; Varas, D.; Loya, J.A.; Zaera, R. Analytical modelling of high velocity impacts of cylindrical projectiles on carbon/epoxy laminates. *Compos. Part A Appl. Sci. Manuf.* **2009**, *40*, 1223–1230. [CrossRef]
24. Harding, J.; Welsh, L.M. A tensile testing technique for fibre-reinforced composites at impact rates of strain. *J. Mater. Sci.* **1983**, *18*, 1810–1826. [CrossRef]
25. Naresh, K.; Shankar, K.; Rao, B.S.; Velmurugan, R. Effect of high strain rate on glass/carbon/hybrid fiber reinforced epoxy laminated composites. *Compos. Part B Eng.* **2016**, *100*, 125–135. [CrossRef]
26. Hou, J.P.; Ruiz, C. Measurement of the properties of woven CFRP T300/914 at different strain rates. *Compos. Sci. Technol.* **2000**, *60*, 2829–2834. [CrossRef]
27. Zarei, H.; Brugo, T.; Belcari, J.; Bisadi, H.; Minak, G.; Zucchelli, A. Low velocity impact damage assessment of GLARE fiber-metal laminates interleaved by Nylon 6,6 nanofiber mats. *Compos. Struct.* **2017**, *167*, 123–131. [CrossRef]
28. Raimondi, L.; Salvi, L.; Semprucci, F.; Falaschetti, M.P. Modelling and Validation of Progressive Damage in Hybrid CFRP–Elastomer Laminates Under Quasi-Static Indentation Loading. *Appl. Sci.* **2025**, *15*, 9284. [CrossRef]
29. Hang, C. Response and Failure Mechanism of 3D Woven Composite Panels Subjected to High Velocity Impact. Doctoral Dissertation, Northwestern Polytechnical University, Xi'an, China, 2023.
30. Hang, C.; Cui, H.; Liu, H.; Suo, T. Micro/meso-scale damage analysis of a 2.5D woven composite including fiber undulation and in-situ effect. *Compos. Struct.* **2021**, *256*, 113067. [CrossRef]

Disclaimer/Publisher's Note: The statements, opinions and data contained in all publications are solely those of the individual author(s) and contributor(s) and not of MDPI and/or the editor(s). MDPI and/or the editor(s) disclaim responsibility for any injury to people or property resulting from any ideas, methods, instructions or products referred to in the content.